Anal. Chem. **1998,** *70,* 2459−2467

Articles

Imaging of Pressure- and Electrokinetically Driven Flows through Open Capillaries

P. H. Paul,* M. G. Garguilo, and D. J. Rakestraw

Sandia National Laboratories, Livermore, California 94550

A new tool for imaging both scalar transport and velocity fields in liquid flows through microscale structures is described. The technique employs an ultraviolet laser pulse to write a pattern into the flow by uncaging a fluorescent dye. This is followed, at selected time delays, by flood illumination with a pulse of visible light which excites the uncaged dye. The resulting fluorescence image is collected onto a sensitive CCD camera. The instrument is designed as an oil immersion microscope to minimize beam steering effects. The caged fluorescent dye is seeded in trace quantities throughout the active fluid, thus images with high contrast and minimal distortion due to any molecular diffusion history can be obtained at any point within the microchannel by selectively activating the dye in the immediate region of interest. We report images of pressure- and electrokinetically driven steady flow within round cross section capillaries having micrometer scale inner diameters. We also demonstrate the ability to recover the velocity profile from a time sequence of these scalar images by direct inversion of the conserved scalar advection−convection equation.

The flow of fluids through microchannels is the basis for many high-performance separation techniques such as high-pressure liquid chromatography, capillary zone electrophoresis, and capillary electrokinetic chromatography. Optimization of these techniques requires an understanding of fluid mechanics and scalar transport within structures having characteristic dimensions of several to hundreds of micrometers. More complex microfabricated fluid systems raise new issues of optimal fluid control, minimization of dead volumes, and enhancing or retarding scalar mixing. Such 3-D devices allow for microchemical reaction chambers, sample injection, gradient elution chromatography, and general fluid handling in an unlimited number of different configurations that offer the potential for improvements in separation efficiency and performance. In the following, we describe a laser-based diagnostic technique that is designed to provide images of both scalar and velocity fields in microchannel liquid flows.

Several different approaches have been taken to image flows through microchannels. Taylor and Yeung[1] seeded the flow with fluorescent latex microspheres. They imaged the short streaks produced by the fluorescence from these particles when the moving flow was illuminated with CW laser light for approximately 1 s. The length and direction of the streaks were then used to infer the vector velocity field and thus to obtain velocity profiles for pressure- and electrokinetically driven flow. One difficulty encountered in using dielectric particles as a tracer in electrokinetic liquid flows is the distinction between electroosmotic and electrophoretic forces acting on the particles as well as the local field gradients and fluid forces generated by polarizable or charged particles in a strong electric field. These effects complicate the image interpretation and require additional experiments to determine bulk flow velocities. To determine the electrophoretic velocity of the particles, Taylor and Yeung employed fluorescence imaging of a dye tracer from which they measured an electroosmotic flow velocity of 0.182 mm/s (as scaled for 30 V/cm at pH 7). They report a total particle velocity of 0.059 mm/s and thus a net particle electrophoretic particle velocity of −0.123 mm/s (from negative to positive at 30 V/cm at pH 7). For an electroosmotic flow they also observed a small velocity defect in the center of the capillary which they attributed to particle-induced viscous drag on the flow.

When using particle tracers it is necessary to avoid conditions where there is a substantial velocity gradient across the particle. For example, in parabolic pipe flow the velocity profile is purely axial; however, a finite value of relative shear across the particle will create a radial motion which may be interpreted as a radial velocity component. Minimizing such effects requires a relative shear across the particle of

$$\Delta u/u = 2rD/(R^2 - r^2) \ll 1$$

(where u is the axial velocity, D is the particle diameter, r is the radial position, and R is the radius of the capillary). This condition is difficult to satisfy near the capillary wall except with very fine particles. The need for submicrometer particles essentially precludes the use of elastic scattering and requires the use of fluorescent particles, as done by Taylor and Yeung, to achieve sufficient signal strength. Another difficulty arises in the interpretation of particle streak images in diverging (converging) flows where the particles move in and out of the image plane during exposure. Finally, it is not possible to use particle tracers to image flow through systems having a dense internal geometry (e.g., a

(1) Taylor, J. A.; Yeung, E. S. *Anal. Chem.* **1993**, *65*, 2928−2932.

S0003-2700(97)00966-9 CCC: $15.00
Published on Web 05/22/1998

packed column) in that the particles will be effectively filtered out.

A number of examples of flow imaging have employed the introduction of a constant stream or plug of dye into capillaries as a means to image the zone front.[1−3] The use of a dye allows imaging of flow through gel-filled,[4] particle-packed, and open microchannel systems. Such techniques have also been applied to study flows through micromachined channels on planar substrates and to evaluate different injection schemes for on-chip analysis and valveless pumping. The main disadvantage of this method is that the leading edge of the dye plug becomes blurred by diffusion, making accurate identification of the front difficult and possibly washing out finer details of the flow structure. This problem is particularly detrimental when the location of interest in the flow system is not in close proximity to a convenient dye injection point. In addition, the nature of the dye injection process can result in a nonideal initial condition as discussed by Tsuda et al.[3] Nonetheless, imaging of the flow of marked fluids during on-chip injection has led to improved injection techniques and devices.[5−7]

Other techniques involving NMR[8,9] and X-ray[10] imaging have also been applied to study flow through fine channels. NMR imaging of electrokinetic flow has been demonstrated in tubes having inner diameters larger than 3 mm. NMR can provide a 3D image of the flow with a reported spatial resolution on the order of 10 μm.[8,9] X-ray imaging of flow through channels of 640 μm diameter has been performed using an oil−water emulsion as the working fluid (with oil droplets of order 1 μm in diameter).[10] The flow field is recovered by double-pulse imaging and speckle velocimetry. This imaging technique has the ability to view flow through channels that are not optically accessible and can provide imaging in 3D geometries, but it requires an emulsion of two media having different refractive indices at X-ray wavelengths. This method is not practical in the study of electrophoresis or chromatography where the mobile phase consists of solvents of similar index and where a heavy loading of dielectric spheres can modify the electric field and hence the flow.

There is a need for complimentary imaging techniques that provide access to both the scalar and velocity fields in microchannel flows. The present work is derived from the flow visualization techniques developed by Lempert et al.[11] The method employs a photoactivatable fluorescent dye tracer, which is initially in a nonfluorescent caged state. This dye can be irreversibly converted to one that will fluoresce following exposure to ultraviolet (UV) light which photocleaves the caging moieties that serve to quench the fluorescence of the original dye. Relatively small amounts of the dye are required because the dye is initially nonfluorescent, hence the imaging is dark-field, and because the dye has a high quantum yield after uncaging. In the experiments reported here, a laser pulse at 355 nm is used to write a pattern into a liquid flow by uncaging some of the dye added as a tracer. After a selected time delay, a short pulse of light from a second blue wavelength laser excites the uncaged dye and the resulting fluorescence image is collected on a CCD camera. Images collected at a series of time delays following uncaging represent the convection and diffusion of the uncaged dye (a conserved scalar). Since a pattern can be written anywhere in the microchannel, the flow can be recorded with limited distortion due to molecular diffusion. Caged dyes are available with a range of molecular structure and charge, thus it should be possible to study diffusion effects as well as the transport of charged versus neutral species in electrokinetic flow. Here, we report the application of this method to obtain time series images of scalar transport in pressure- and electrokinetically driven flow in open fused silica capillaries. We also describe a means to obtain velocity profiles from these data and demonstrate the method as applied to steady parabolic pipe flow.

EXPERIMENT

Imaging Diagnostic Tool. Figure 1 shows a schematic diagram of the imaging system. The uncaging step was performed using 355 nm light from a tripled Nd:YAG laser (nominal 5 ns pulse). The 355 nm light was spatially filtered with a 25 μm slit and then focused with a single 10 cm focal length lens to produce a sheet having a thickness of ∼20 μm and a width of ∼500 μm (wider than the inner diameter of the microchannel). The plane of this sheet was oriented perpendicular to the axis of and directed to section the capillary. The total 355 nm energy at the capillary was less than 100 μJ. A second CW laser (5−10 mW) was used to excite the uncaged dye (the first instrument employed a 488 nm argon ion laser, the present instrument employs a 473 nm frequency doubled Nd:YVO_4 laser). The CW blue light was converted to a variable duration pulse by shuttering the beam with a combination of a ferroelectric rotator and a Glan-Taylor polarizer. The blue light was directed through a microscope objective to flood illuminate the region of interest (approximately 300 μm of capillary length). This same objective was used to collect the fluorescence image through a dichroic beam splitter (488 nm reflecting and 550 nm long-pass transmitting) which was also used as a turning mirror for the blue laser. The fluorescence was further spectrally filtered (500 nm long pass) before being imaged onto a CCD array (11 mm diagonal) operating in a RS-170 video mode. The data from the CCD camera was fed to a monitor for real-time viewing and to a PC-based frame grabber for data acquisition.

The microscope objective and focusing mount, the beam splitter and filter, the polarizer and ferro-rotator, the 473 nm laser and beam shaping optics, and the CCD camera were all mounted as a single assembly. This assembly was mounted on a precision three-axis stage which was suspended over the work piece to provide ease of alignment and access to the microchannel. The microchannel was mounted on a separate precision three-axis stage. The uncaging beam was directed to the work piece from

(2) Kuhr, W. G.; Licklider, L.; Amankwa, L. *Anal. Chem.* **1993**, *65*, 277−282.
(3) Tsuda, T.; Ikedo, M.; Jones, G.; Dadoo, R.; Zare, R. N. *J. Chromatogr.* **1993**, *632*, 201−207.
(4) Fujimoto, C.; Fujise, Y.; Matsuzawa, E. *Anal. Chem.* **1968**, *68*, 2753−2757.
(5) Jacobson, S. C.; Hergenroder, R.; Koutny, L. B.; Warmack, R. J.; Ramsey, J. M. *Anal. Chem.* **1994**, *66*, 1107−1113; *Anal. Chem.* **1994**, *66* 3472−3476.
(6) Seiler, K.; Fan, Z. H.; Fluri, K.; Harrison, D. J. *Anal. Chem.* **1994**, *66*, 3485−3491.
(7) v-Heeren, F.; Verpoorte, E.; Manz, A.; Thormann, W. *Anal. Chem.* **1996**, *68*, 2044−2053.
(8) Manz, B.; Stilbs, P.; Jonsson, B.; Sodermann, O.; Callaghan, P. T.; J., *Phys. Chem.* **1995**, *99*, 11297−11301.
(9) Wu, D.; Chen, A.; Johnson, C. S.; Magn., J. *Resonance Ser. A* **1995**, *115*, 123−126.
(10) Lanzillotto, A.-M.; Leu, T.-S.; Amabile, M.; Wildes, R.; Dunsmuit, J. An investigation of microstructure and microdynamics of fluid flows in MEMS. *Proc. ASME Aerospace Division AD-52* **1996**, 789−795.
(11) Lempert, W. R.; Magee, K.; Ronney, P.; Gee, K. R.; Hauglan, R. P. *Exp. Fluids* **1995**, *18*, 249−257.

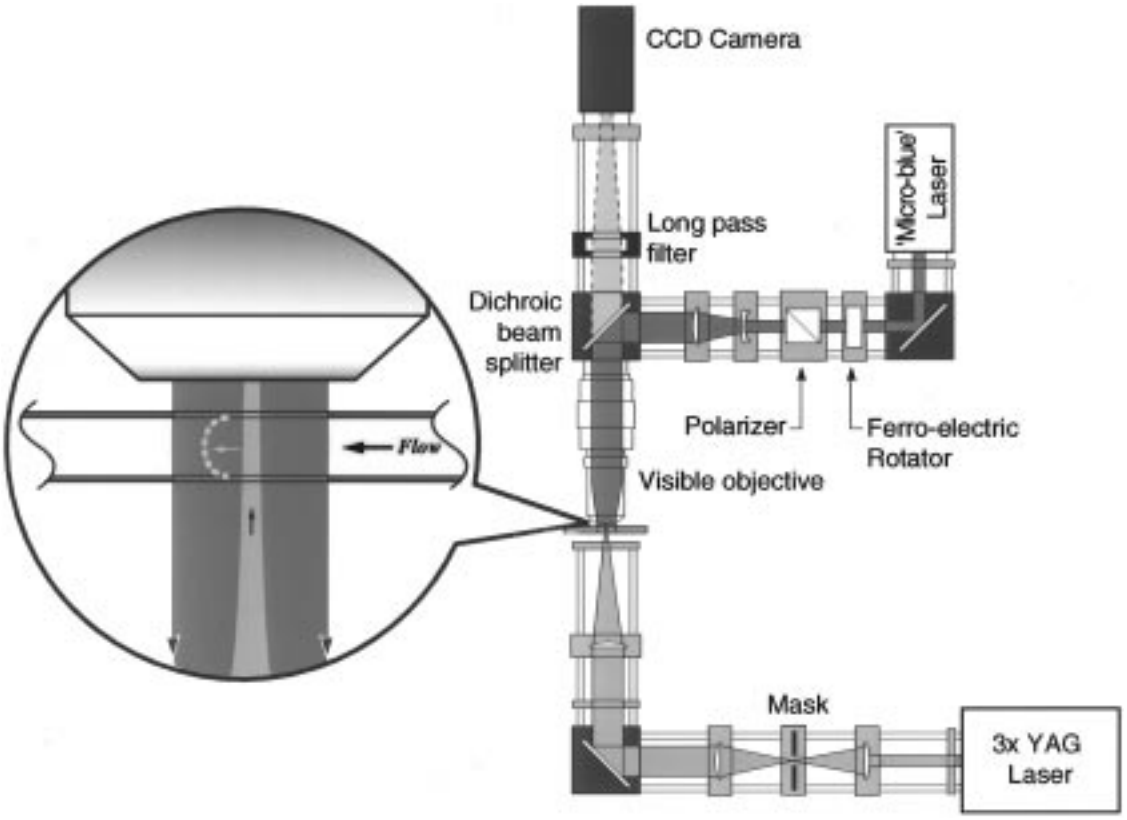

Figure 1. Schematic diagram of the microflow imaging instrument.

below. Oil immersion of the capillary between two flat quartz microscope slides was employed to minimize beam steering effects due to the curved walls of the capillary. The immersion oil had high viscosity, low fluorescence, and an index of 1.51 which provides a reasonable match to the index of fused silica and the typical fluids within the capillary.

Image Acquisition. To maintain stable operation of the YAG laser it is necessary to fire the lamps at 10 Hz; however, the video camera operates at 30 frames/s. The actual uncaging/imaging rate ranges from 1/s to as slow as 1/min to allow the uncaged dye to fully leave the viewing region prior to starting the next uncaging/imaging cycle. We employ a custom-built RS-170 video sync generator as the master oscillator. This is followed by a series of thumbwheel programmable counters to provide (1) a 10 Hz YAG lamp trigger; (2) a synchronized programmable hold-off for the YAG Q-switch trigger, which can be immediate with the lamps to one Q-switch trigger per 1024 lamp triggers; and (3) a similar synchronized programmable counter for the ferro-rotator and frame grabber triggers. In this fashion, the computer waits to acquire the one video frame which contains the image data (the other frames being dark). The RS-170 composite sync from the generator is used to genlock the camera and the frame grabber.

An RS-170 video frame is composed of two image fields, which represent separate images each having a $^1/_{60}$ s exposure. Since the dye fluorescence is prompt, the actual exposure time is controlled by the open-time of the ferro-rotator. The system can be operated in three modes: (1) the ferro-rotator is set open which allows the entire process to be viewed in real time, this mode is used for alignment and direct videotaping; (2) the delay of the ferro-rotator open-time is stepped in $^1/_{30}$ s intervals using the programmable counters, this mode is used to map out the long-term (large-scale) time evolution of the flow; and (3) the programmable delay for the ferro-rotator open-time is fixed and the delay is adjusted in fine steps of approximately 1 ms using an SRS pulse generator, this mode is used to acquire a high temporal resolution scalar image sequence that is required for inversion to a velocity image. The SRS pulse generator is also used to set the ferro-rotator pulse width and hence the temporal width of the exposure. For data acquisition, exposure widths ranging from 1 to 10 ms were used, as required to balance signal level at the camera against motional blurring. The as-acquired image is composed of 240 by 384 pixels with a size of 24×24 μm, e.g., corresponding to a 2.4 μm sample size in the flow with a 10× objective.

Fluorescence images were collected using single pulses of UV light and for selected time delays of blue light. The images were corrected in postprocessing by subtraction of a dark frame and normalization with a white frame. The dark frame was obtained by blocking the UV laser and recording a background image due to any ambient light leakage and camera pixel-to-pixel offset variations. The white frame was obtained by stopping the flow in the capillary and overexposing the fluid to UV light to generate a significant amount of uncaged dye which was then allowed to diffuse in the absence of the UV light and in the stagnant flow. An image of this condition provided a normalization that removes any nonuniformities in the blue laser illuminating beam or response nonuniformities in the imaging system. The dark and white field corrections and any other image processing were performed using the Khorus image processing package running on a Sun workstation.

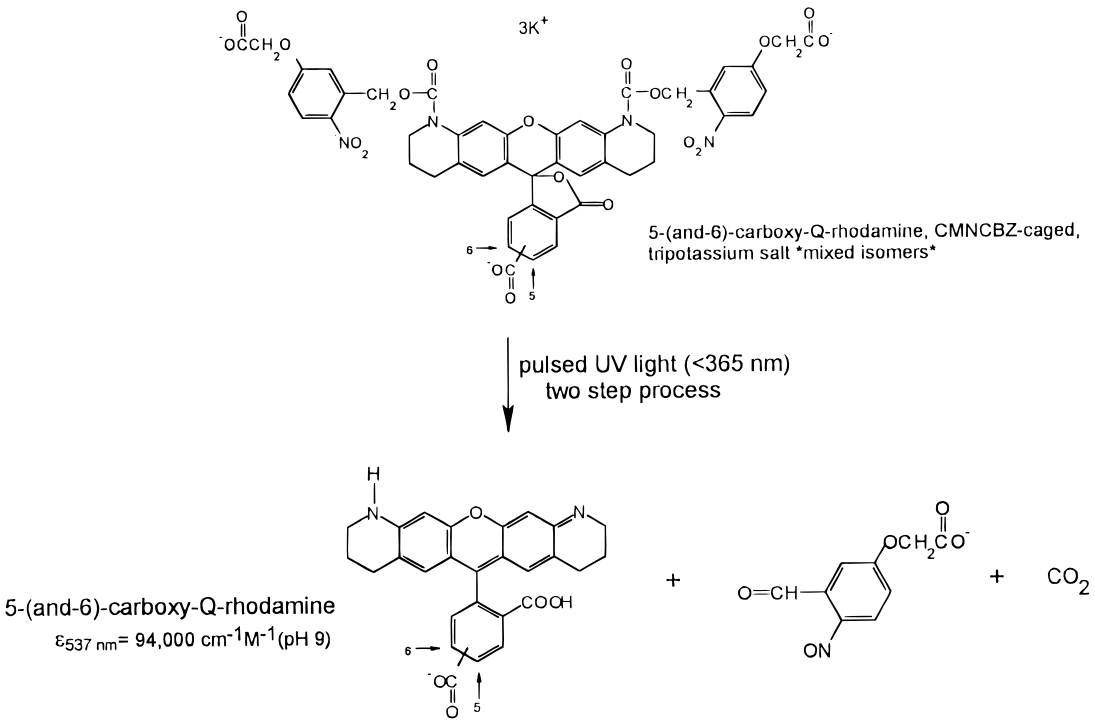

Figure 2. Structure of CMNCBZ-caged 5-(and-6)-carboxy-Q-rhodamine dye (top) and uncaged 5-(and-6)-carboxy-Q-rhodamine dye (bottom).

Capillary Flow System. The capillaries were mounted on a three-axis stage using modified fiber optic holders which consisted of a metal base with groove guides and magnetic clamps. A detection window was created by stripping 2−5 mm of the polyimide cladding away from the fused-silica capillary using a thermowire stripper. For all of the experiments, the capillary was flushed and filled with a stock solution of an appropriate caged dye. One end of the capillary was placed in an inlet reservoir which contained the stock dye solution. The other end was placed in an outlet reservoir which contained only a solution of the buffer. Pressure-driven flow was generated by elevating the inlet reservoir approximately 5 cm with respect to the outlet reservoir. Electrokinetic flow was generated by applying a high-voltage dc electric field along the capillary between platinum electrodes placed in the solution in each of the reservoirs. For the electrokinetic studies, the heights of the two reservoirs were carefully balanced to prevent any pressure-driven flow due to gravity.

Chemical and Materials. 4,5-Dimethoxy-2-nitrobenzyl (DMNB)-caged fluorescein dextran (10 000 MW, anionic) and ((5-carboxymethoxy-2-nitrobenzyl)oxy)carbonyl (CMNCBZ)-caged 5-(and-6)-carboxy-Q-rhodamine (tripotassium salt, mixed isomer, and succinimidyl ester) dyes were used as supplied by Molecular Probes. Figure 2 shows the structures of CMNCBZ-caged 5-(and-6)-carboxy-Q-rhodamine dye (top) and uncaged 5-(and-6)-carboxy-Q-rhodamine dye (bottom). Fused-silica capillary (365 μm o.d.; 75 μm and 100 μm i.d.) was purchased from Polymicro Technologies. Acetonitrile (ACN) was used as supplied by Aldrich. Sodium carbonate and tris(hydroxymethyl)aminomethane (TRIS) were used as supplied by Sigma. The water used was purified with a Labconco Ultrapure water system. Stock solutions of the DMNB-caged fluorescein dextran dye were prepared by dissolving 5 mg of the as-received solid in a 3 mL solution of 0.1 M sodium carbonate buffer, pH 9.0. Stock solutions of the CMNCBZ-caged 5-(and-6)-carboxy-Q-rhodamine dye were prepared by dissolving 1 mg of the as-received solid in a 0.5 mL solution of 70% ACN and 30% 5 mM TRIS buffer, pH 8.0. The stock solutions were stored under cool, dark conditions to minimize uncaging of the dyes.

RESULTS AND DISCUSSION

Pressure-Driven Flow. Figure 3 shows a set of images of steady, fully developed, pressure-driven flow through a 100 μm i.d. capillary. The first frame is taken at $t \equiv 0$ (the time the UV light pulse was applied) and represents the initial distribution of the uncaged dye. The two-dimensional image of the initial distribution appears as a straight line with a near-Gaussian width of ~20 mm which is currently limited by the UV laser sheet optics. The field of view and focus of the microscope were adjusted to collect the image from the center plane of the capillary. Subsequent frames represent the evolution of the initially uncaged dye as dictated by convection and diffusion. As expected, the fluid near the walls appears stagnant while the most rapid displacement occurs on the center line. In this case the velocity is purely axial and has a radial profile of the form

$$u(r) = u_p(1 - (r/R)^2)$$

where u_P is the center line velocity. This is often called parabolic or Hagen−Poiseuille pipe flow. The condition of creeping flow occurs for values of $\mathrm{Re} = 2Ru_p/\zeta$ less than unity where η is the kinematic viscosity (in the present case, Re ≈ 0.1). Flow in this limit implies a condition where viscous drag completely dominates inertial forces.

Consider the case of a Gaussian profile mark, as written into the flow, of the form

$$C(t = 0,r,z) = \exp(-(z/\sigma)^2) \qquad (1)$$

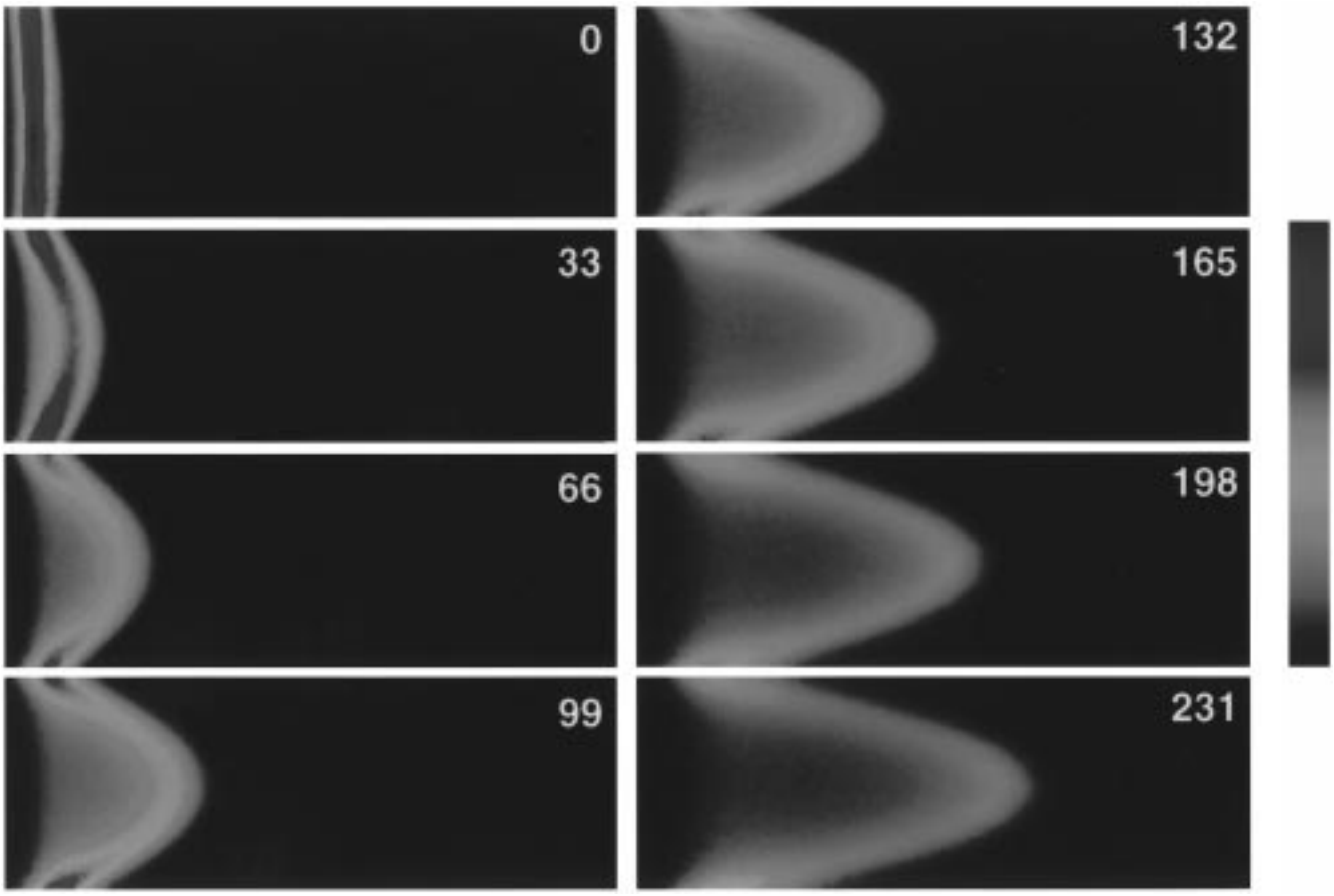

Figure 3. Images of pressure-driven flow through an open 100 μm i.d. fused-silica capillary using a caged fluorescein dextran dye. Pressure differential of 5 cm of H_2O per 60 cm of column length. Viewed region 100 by 200 μm. The frames are numbered in ms as measured from the uncaging event.

where C is the concentration of the uncaged dye and z is axial position. For an incompressible flow, the equation of motion for the mark (the conserved scalar advection−convection equation) is

$$\frac{\partial C}{\partial t} + \vec{u}\cdot\nabla C = D\nabla^2 C \qquad (2)$$

where D is the diffusion coefficient of the dye. In the limit of negligible diffusion this has the solution

$$C(t,r,z) = \exp(-(z - u(r)t)^2/\sigma^2) \qquad (3)$$

The parabolic velocity profile can be recovered from the differential motion in time of the locus of the maxima in the axial direction. Alternatively, the velocity profile can be obtained by processing two images taken at a sufficiently small separation in time, δt, via

$$u(r) \simeq (C(t_0 + \delta t) - C(t_0))/\nabla C(t_0) \qquad (4)$$

However, such a simple relation between the scalar image(s) and the velocity field is not the general case, particularly in the presence of strong diffusion or for multidimensional flows. Rather, the velocity field must be recovered by using a time series of scalar images to invert the equation of motion, which yields a unique solution for 2D steady incompressible flow. The condition of incompressibility provides the second equation for the velocity field, i.e.,

$$\nabla\cdot\vec{u} = 0$$

This technique, termed scalar imaging velocimetry (SIV), has been developed and applied to the more general problem of turbulent 3D flows by Dahm and co-workers.[12]

We have applied the SIV method to data obtained for pressure-driven flow in an open capillary. The SIV method requires an iterative solution for the components of the vector velocity field. The initial seed for the SIV data reduction was taken as the velocity profile obtained under the assumption of negligible mass diffusion (i.e., as given by reducing the concentration data according to eq 4). Figure 4 shows three velocity profiles as recovered from three different image pairs using the SIV method for pressure driven flow in a 100 μm i.d. capillary using caged fluorescein dextran dye in water buffered to pH 9. The raw data was recorded using a blue laser pulse length of 1 ms and a time delay between frame pairs of 20 ms. The image pairs were acquired by double pulsing the ferrorotator to record the two images on the two fields of a

(12) Dahm, W. J.; Su, L. K.; Southerland, K. B. *Phys. Fluids A* **1992**, *10*, 2191−2206.

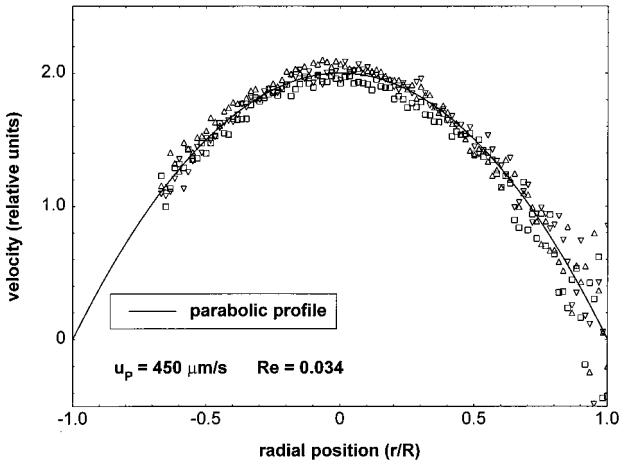

Figure 4. Three SIV velocity profiles (points) recovered from three image pairs for pressure-driven flow in a 75 μm i.d. open capillary. A parabolic profile (line) is also shown for comparison. Velocity data were not recovered for $-1 < r/R < -0.5$ due to poor signal-to-noise in the data.

single video frame. The measured velocity profile is well represented by a parabola (also shown in Figure 4). However the scatter in the measurements becomes quite large near the walls. This is the result of trying to recover a vanishing velocity (near the wall) in the presence of diffusion and of finite noise in the images. To be able to measure lower velocities requires both larger time delays between the image pairs and frame averaging of the inversion results to improve the signal-to-noise ratio.

Electrokinetic Flow. Figure 5 shows an image series obtained for electrokinetically driven flow through an open 75 μm i.d. capillary. In this case, a caged rhodamine dye was employed. As in the pressure-driven case, the first frame is taken at $t \equiv 0$ and represents the initial distribution of the uncaged dye. The subsequent images show a plug-like scalar flow, and hence implies a plug-like velocity profile. Over the entire time period (some 165 ms), the measured cross stream profiles remain relatively flat and show a relatively uniform signal intensity (wall to wall). In this flow, the fluid is driven through the capillary by the electroosmotic flow generated by the applied field acting on the charge double layer at the capillary wall. Rice and Whitehead[13] give a relation for the electrostatic potential, ϕ, due to the charge distribution in capillary electrokinetic flow of the form

$$\frac{1}{r}\frac{\partial}{\partial r} r \frac{\partial \phi}{\partial r} = \frac{k_B T}{e} \kappa^2 \sinh(e\phi/k_B T) \qquad (5)$$

where κ is the Debye length. The potential is subject to boundary conditions of axial symmetry and of $\phi = \phi_0$ at the wall. Substitution of eq 5 into the momentum equation for incompressible flow, at small Reynolds number and subject to conditions of axial symmetry and no-slip at the wall (i.e., $u = 0$ at the wall), yields

$$u(r) = u_E(1 - \phi(r)/\phi_0) + u_P(1 - r^2/R^2) \qquad (6)$$

Here $u_{(E)} \equiv -E_z(\epsilon\phi_0/\mu)$ and $u_P \equiv -P_z(R^2/4\mu)$ where E_z and P_z are the axial electric field and pressure gradient and μ is the dynamic viscosity. A solution to eq 5 can be found in terms of modified Bessel functions,[13] which is appropriate for values of $e\phi_0/k_BT$ less than unity. In this limit and for large values of κR, the mean velocity is given by $u_M = u_E + u_P/2$.

Outside of the double layer $\phi(r)/\phi_0$ goes to zero (i.e., for $r < R$, $\phi(r)/\phi_0 \rightarrow 0$ for κR large) in which case the velocity profile is a superposition of a constant electroosmotic velocity and a parabolic flow. The data shown in Figure 5 were obtained by first establishing a zero pressure gradient condition in the absence of an applied field. The resulting flow displays pure electrokinetic behavior within the resolution of the technique. It was necessary to employ a well-filtered fluid to achieve this result. Early experiments, using as-dissolved dyes, displayed slight parabolic behavior (a value u_P/u_E of order 10%). This secondary parabolic component was likely the result of drag on the fluid produced by electrophoretic forces on the suspended particles (as described by Taylor and Yeung) or continuity conditions which require a constant product of $\rho u_M A$ (where A is the cross-sectional area and ρ is the fluid density) along the entire length of the capillary. As such, any partial blockage of the capillary, due to a particle deposit anywhere along the length, will introduce a negative pressure gradient and thus a concave parabolic front. The data of Figure 5 suggest that a pure electrokinetic profile can be achieved for a particle-free flow in an unobstructed channel. There are other secondary nonideal processes which can induce a parabolic flow component, such as positive axial temperature gradients due to ohmic heating which accelerate the flow and thus introduce a convex parabolic front, or temperature-induced variations in the viscosity (radial and axial) which may introduce a parabolic front of either sign. The imaging results suggest that such thermal effects introduce negligible flow distortions under the present flow conditions.

Several important parameters can be extracted from this type of image data, including diffusion coefficients, drift velocities, and the relative contribution of pressure and electrokinetic forces. Figure 6 shows signal profiles taken along axial cuts at different times after the write event. As expected, the peak values decrease and widths increase due to mass diffusion. For near flat velocity and scalar profiles and a purely axial electric field, the continuity equation takes the form

$$\frac{\partial C}{\partial t} + (u_E + u_{ph})\frac{\partial C}{\partial z} = D\frac{\partial^2 C}{\partial z^2} \qquad (7)$$

Here $u_{ph} = v_{ph}E_z$ is the ion drift velocity of a charged dye, where v_{ph} is termed the electrophoretic mobility of the dye. The apparent velocity in the images is thus a sum of convective and ion drift velocities. Equation 7 has been applied to the data to obtain values of $u_E + u_{ph} \approx 390 \pm 20$ μm/s at an applied field of 200 V/cm, and $D = 6.3 \times 10^{-6}$ cm^2/s for the uncaged rhodamine dye in ACN (80%) Tris-buffered (pH 8) at 20 °C. The electrophoretic mobility can be estimated using the measured diffusion coefficient and the Nernst−Einstein relation, giving $v_{ph} \approx -2.46 \times 10^{-4}$ cm^2 V^{-1} s^{-1}. It is common to define an electroosmotic mobility in the form $v_E = u_E/E_z$ which can then be estimated from the measured apparent velocity of the dye, giving $v_E \approx 4.4 \times 10^{-4}$ cm^2 V^{-1} s^{-1}.

(13) Rice, C. L.; Whitehead, R. J. *J. Phys. Chem.* **1965**, *69*, 4017−4024.

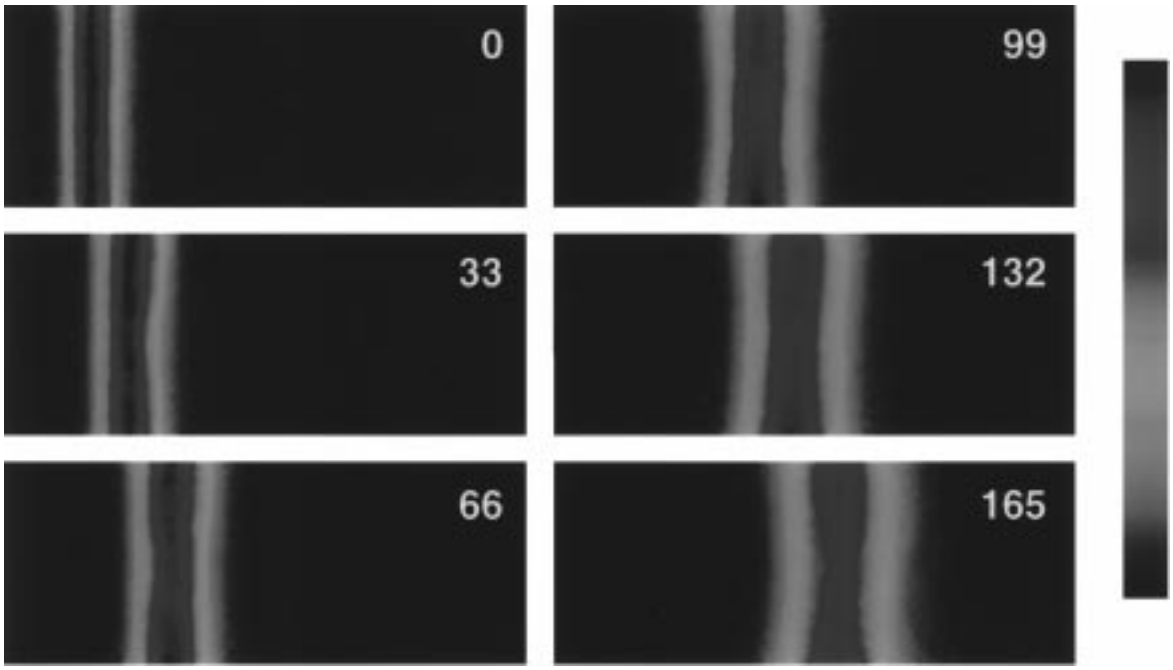

Figure 5. Images of electrokinetically driven flow through an open 75 μm i.d. fused-silica capillary using a caged rhodamine dye. Applied field of 200 V/cm. Viewed region 75 by 188 μm. The frames are numbered in milliseconds as measured from the uncaging event.

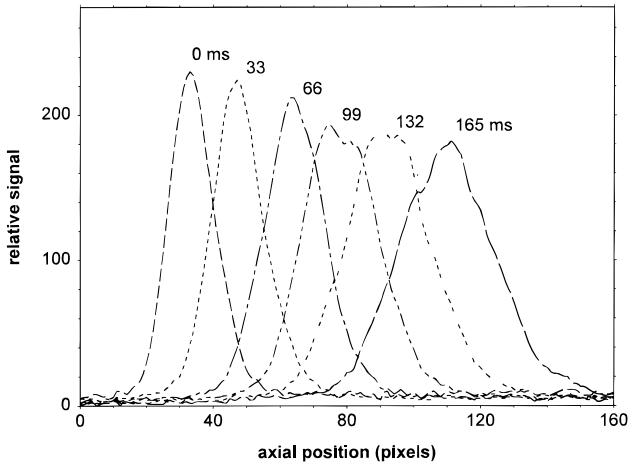

Figure 6. Plots of signal intensity vs axial distance taken from the images of Figure 5. The curves are labeled with time measured from the uncaging event.

Figure 7 shows a set of images of electrokinetic flow through an open 100 μm i.d. capillary using a buffer solution seeded with a nominally pure caged fluorescein dextran dye. These images and the axial signal profiles plotted in Figure 8 show the generation of multiple bands owing to the actual multicomponent nature of this dye. The solution contained free caged fluorescein (MW = 440) and dextrans with one or two caged fluoresceins attached. The dextrans themselves consisted of a molecular weight distribution that ranges from approximately 8000 to 12000. This complex mixture is separated electrokinetically during the experiment. We believe that the narrow band on the left in the images is the pure fluorescein and the broader two bands proceeding to the right are dextrans with two and one fluorescein attached, respectively. The apparent broadening of the two dextran bands is the result of electrokinetic separation of the range of charge-to-mass ratio components which does not occur in the pure fluorescein band. The fluorescein dextran was used in the initial pressure-driven experiments (e.g., Figure 3) to reduce diffusion effects, in which case the multicomponent nature of the mixture was of little importance. The impurity of the fluorescein−dextran dye mixture as well as the distribution of molecular weights of the dextran negates any advantages in reduced diffusional broadening for the study of electrokinetically driven flows.

The signal profiles taken from the data of Figure 7 were fit to determine the apparent velocity and broadening coefficients for the three bands. The observed broadening of the pure fluorescein component gave a diffusion coefficient of 4.37×10^{-6} cm^2 s^{-1} which is due to pure mass diffusion. For an uncaged fluorescein dye in water buffered to pH 8, a separate measurement in a stagnant flow gave a diffusion coefficient of 4.22×10^{-6} cm^2 s^{-1}. These values are in reasonable agreement with the value of 4.41×10^{-6} cm^2 s^{-1} reported for fluorescein at pH 6.8 by Moore and Jorgenson.[14] Using the measured diffusion coefficient, the electrophoretic mobility of the uncaged fluorescein is estimated at $v_{ph} \approx -3.3 \times 10^{-4}$ cm^2 V^{-1} s^{-1} and using the measured apparent velocity the electroosmotic mobility is estimated at $v_E \approx 5.07 \times 10^{-4}$ cm^2 V^{-1} s^{-1}. These are in reasonable agreement with the values $v_{ph} = -3.3 \times 10^{-4}$ cm^2 V^{-1} s^{-1} and $v_E = 5.87 \times 10^{-4}$ cm^2 V^{-1} s^{-1} reported by Harrison et al.[15] for fluorescein in pH 8.5 buffer and for fused silica. The mobilities can also be recovered from the data by observing that the electrophoretic velocity of the dextran with two fluoresceins attached is nominally twice that of the dextran with one attached: giving $v_{ph} = -3.2 \times 10^{-4}$ cm^2 V^{-1} s^{-1} for the pure fluorescein, $v_{ph} = -6.5 \times 10^{-5}$ cm^2 V^{-1} s^{-1} for the single fluorescein dextran (and twice that value for the double fluorescein dextran), and $v_E = 4.97 \times 10^{-4}$ cm^2 V^{-1} s^{-1}. Again,

(14) Moore, A. W.; Jorgenson, J. W. *Anal. Chem.* **1993**, *65*, 3550−3560.
(15) Harrision, D. J.; Manz, A.; Fan, Z.; Ludi, H.; Widmer, M. *Anal. Chem.* **1992**, *64*, 1926−1932.

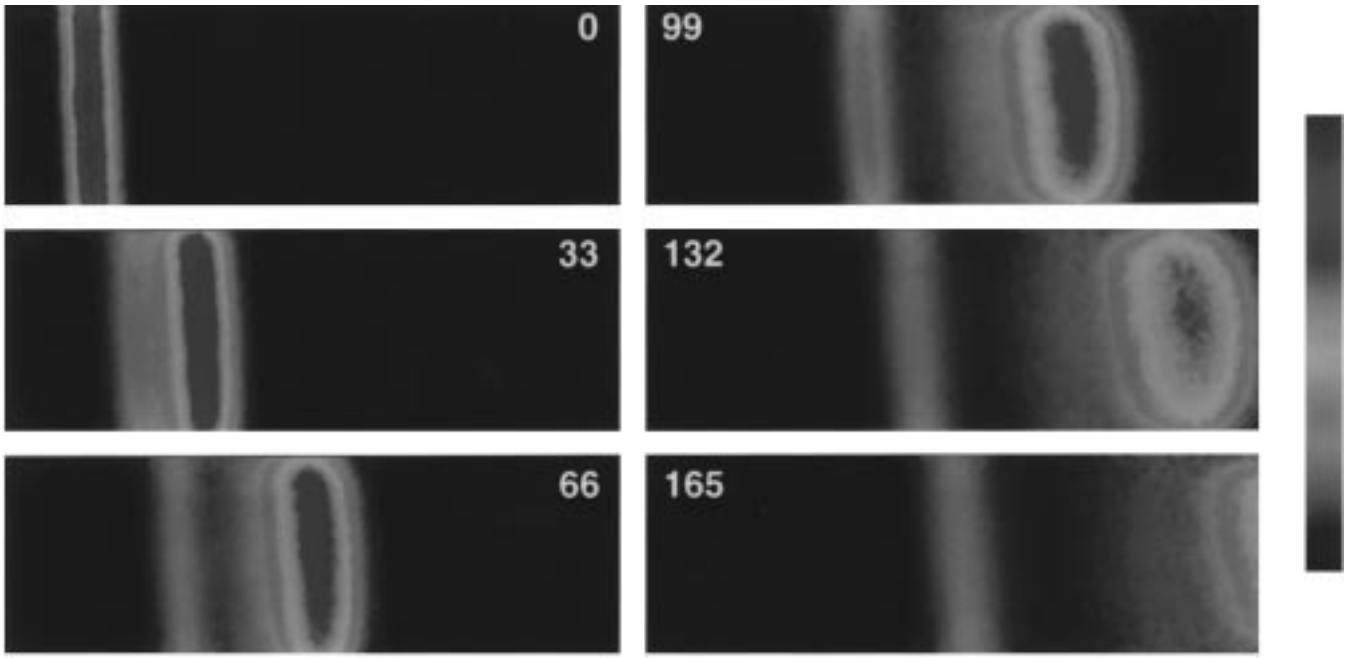

Figure 7. Images of electrokinetically driven flow through an open 100 μm i.d. fused-silica capillary using a caged fluorescein dextran dye. Applied field of 120 V/cm. Viewed region 100 by 300 μm. The frames are numbered in milliseconds as measured from the uncaging event.

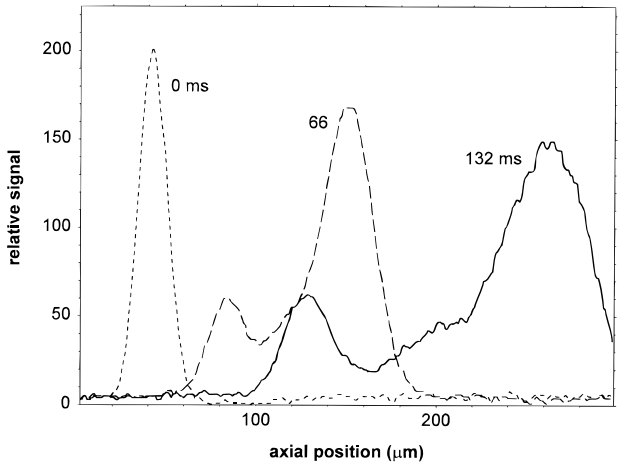

Figure 8. Plots of signal intensity versus axial distance taken from the images of Figure 7. The curves are labeled with time measured from the uncaging event.

these values are in reasonable agreement with the estimates based on measured diffusion coefficients and published results.

Careful examination of the data presented in Figure 7 provides additional details regarding the molecular transport of the various species. In particular, the fluorescein dextran bands are observed to move away from the walls, which is not the case for the pure fluorescein band. The dye molecules are negatively charged, but the charge-to-mass ratio changes dramatically between the fluorescein ($-2/400$) and the dextrans ($-2/10000$ and $-4/10000$). The exact cause for this effect is not understood, but similar behavior has been observed by Tsuda et al.[3] for flow in a rectangular capillary of dimensions 1 mm $\times$ 50 μm. They observed a similar repulsion from the wall for anion species and attributed this to a repulsion by the negatively charged walls of the capillary. They observed the inverse effect for positively charged analytes. These wall effects were amplified in their experiments due to the relatively large width of their channels (1 mm). The observation of such effects over a short time period (here over several hundred milliseconds) points out the sensitivity of the caged dye method as well as the ability to investigate neutral and charged species transport. The observation of these effects also raises a caution regarding the interpretation of electrokinetic flow images without first considering the possible charged nature of the caged dye being used. The most effective use of the imaging technique described here to isolate the electroosmotic flow will require the use of a neutral marker. We are currently attempting to identify an effective caged dye that produces a neutral marker following photolysis.

The spatial resolution of the imaging apparatus described here is approximately 5 μm in the object plane. The use of higher power microscope objectives (10$\times$ in the current experiment) and improved sheet optics for uncaging the dye molecules will result in modest improvement in the object plane resolution. Ultimately, the ability of this technique to extract high-resolution flow field information is limited by the rate of diffusion as compared to the typically slow flow velocities at these small scales. The out-of-plane resolution is more problematic. In the current experiments, we estimate our depth of field to be $\sim$20 μm (10$\times$, 0.3 N.A.). In the case of the electrokinetically driven flows where no substantial out-of-plane variation occurs, this is not an issue. However, the interpretation of images that have substantial out-of-plane variations such as in pressure-driven pipe flow must account for this effect. The application of phase conjugate, confocal, or two-photon fluorescence microscopy could be implemented to improve the depth-of-field resolution of this method.

CONCLUSIONS

We have described an imaging tool for the study of flows in microchannels. This technique is based on a write and read method and thus has the potential to provide sharp high-resolution images with little degradation due to diffusion history. This allows flow imaging to be conducted under steady-state conditions at any

desired location in microfluidic systems, which provides a significant advantage over existing imaging approaches which depend on the injection of a dye slug. In addition, the method provides a direct means to study diffusion effects. The technique was demonstrated for pressure- and electrokinetically driven flows in capillaries. A method to extract the velocity profiles from time sequence image data was presented and applied to pressure-driven parabolic flow. The flow marker employed has molecular dimensions, thus it is possible to apply this technique to study flows within porous structures. The uncaged dye products used in the current study are charged and therefore complicate the interpretation of images obtained in electrokinetically driven flows. A search for uncharged markers is underway. We are currently applying these techniques to the study of flow in packed capillaries as used in electrokinetic chromatography and to flows in microfabricated planar structures.

ACKNOWLEDGMENT

The authors thank Mr. Gary A. Hux and Mr. Herb Blair for their technical assistance, and acknowledge the support of the Sandia Laboratory Directed Research and Development Program.

Received for review September 3, 1997. Accepted April 6, 1998.

AC9709662